

Influence of Metastable Disorder in Titanium Oxyhydroxides on High-Rate Sodium Ion Storage

Dnyanesh Vernekar,^{a†} Soumyajit Gupta,^{a†} Gi-Hyeok Lee,^b Reshma Devi,^c Mohamed Ruwaid Rafiuddin,^d Gopalakrishnan Sai Gautam,^c Wanli Yang,^b Srinivasan Ramakrishnan^{a*}

^aDepartment of Chemistry, Indian Institute of Technology Bombay, Mumbai-400076, India

^bAdvanced Light Source, Lawrence Berkeley National Laboratory, Berkeley, CA 94720,
USA

^cDepartment of Materials, Indian Institute of Science, Bengaluru 560012, India

^dMIAMI facility, School of Computing and Engineering, University of Huddersfield,
Huddersfield HD1 3DH, United Kingdom

*srini@chem.iitb.ac.in

Contents

S. No.	Description	Page Number
1	FWHM comparison between batch sizes	S2
2	Rietveld refinement of the powder X-ray diffraction data	S2
3	Variation of the 'a' and 'c' lattice parameter of the various TiO _x (OH) _y -T _{anneal}	S2
4	Adsorption Isotherms and BJH Pore volume	S3
5	Cl 2p XPS ,Relative Ti ³⁺ :Ti ⁴⁺ ratio and EPR spectra	S4
6	GCD and Rate Capability Tests	S4
7	CVs at different scan rates and the peak fitting to obtain b-values	S5
8	Ex-situ pXRD diffractograms and in-situ Raman spectra	S6
9	Comparative cycling performance of TiO _x (OH) _y -400 after 5 cycles at 13 mA/g	S7

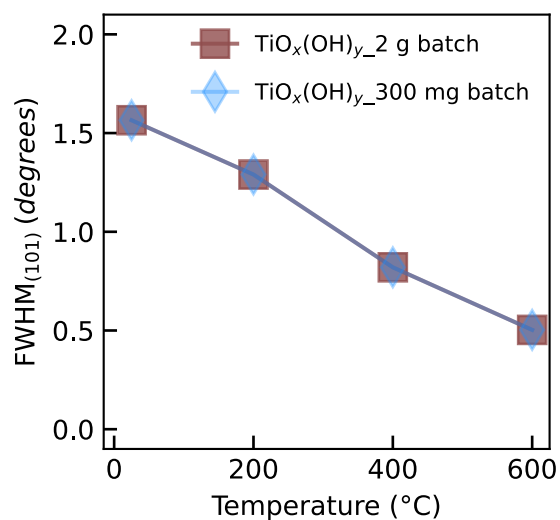


Figure S1. Comparative FWHM of the synthesized $\text{TiO}_x(\text{OH})_y\text{-T}_{\text{anneal}}$ samples across two different batch sizes.

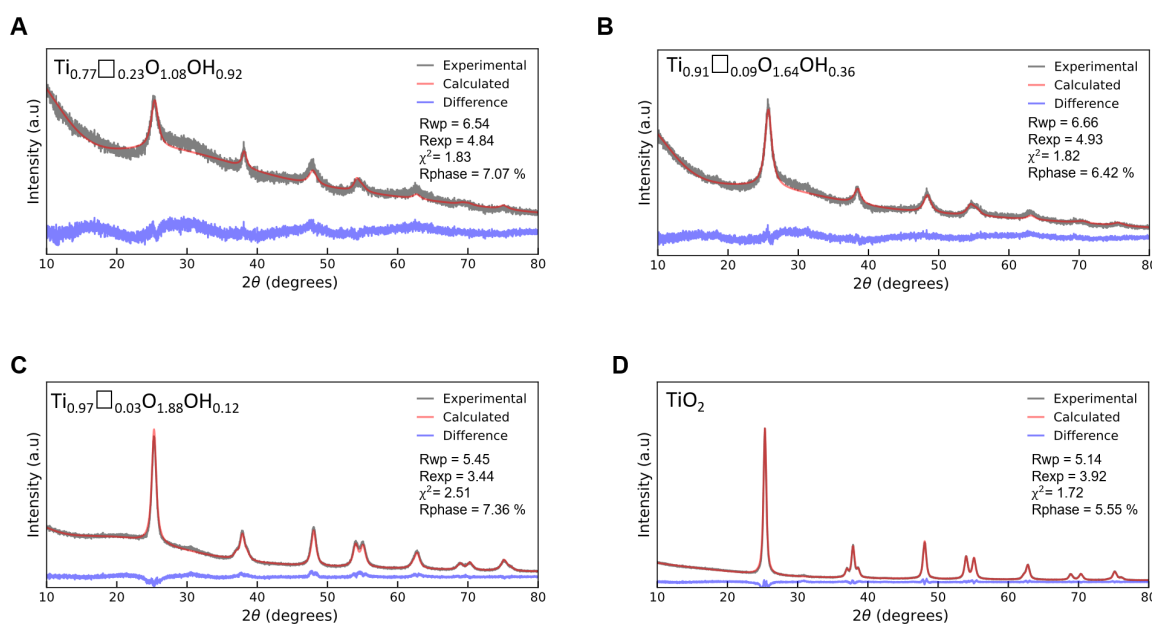


Figure S2. (A)-(D) Rietveld refinement of the powder XRD data of the various $\text{TiO}_x(\text{OH})_y\text{-T}_{\text{anneal}}$ samples. Black, red and blue lines represent the experimental, calculated and difference curves respectively.

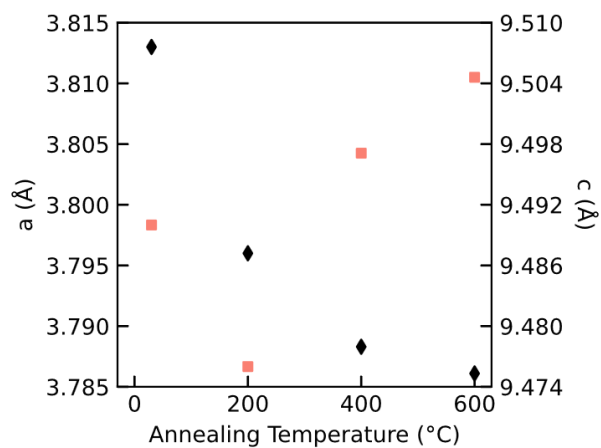


Figure S3. Variation of the 'a' and 'c' lattice parameter of the various $\text{TiO}_x(\text{OH})_y\text{-T}_{\text{anneal}}$, as obtained from the Rietveld refinement.

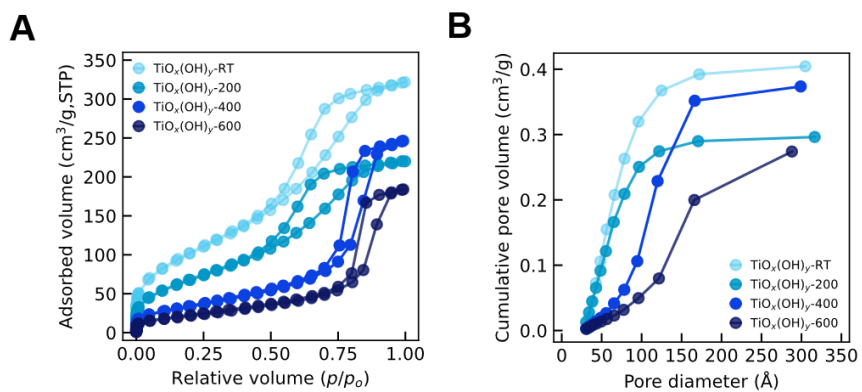


Figure S4. (A) Adsorption isotherms, and (B) pore volume distribution for various $\text{TiO}_x(\text{OH})_y\text{-T}_{\text{anneal}}$ samples.

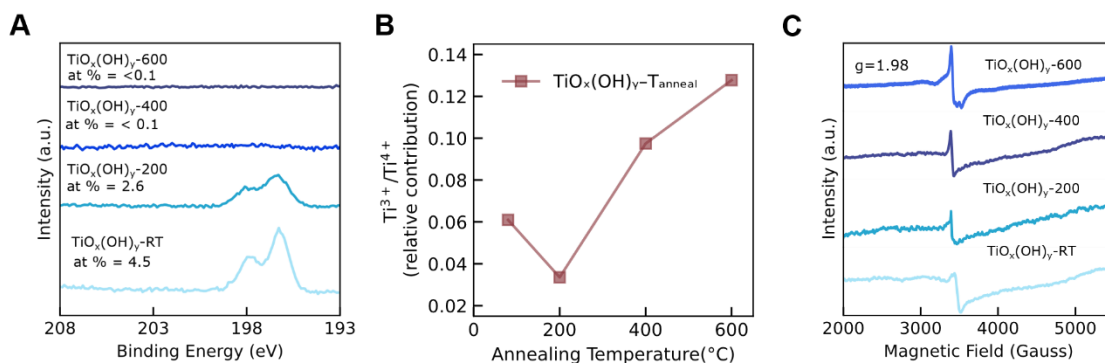


Figure S5. (A) Cl 2p XPS spectra. (B) Relative $\text{Ti}^{3+}:\text{Ti}^{4+}$ ratio obtained from deconvolution of Ti 2p XPS signal. (B) Electron paramagnetic resonance (EPR) spectra for various $\text{TiO}_x(\text{OH})_y\text{-T}_{\text{anneal}}$ samples.

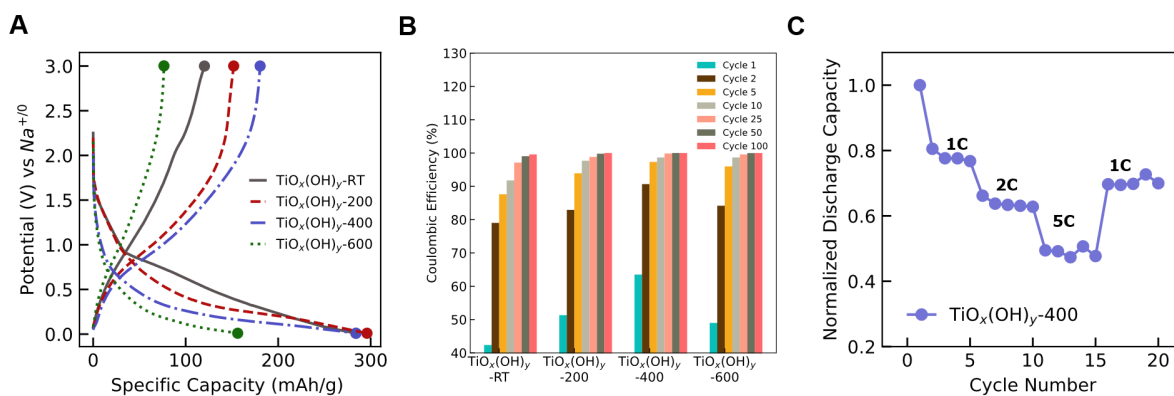


Figure S6. (A) First cycle GCD profiles and (B) coulombic efficiency of various $\text{TiO}_x(\text{OH})_y\text{-T}_{\text{anneal}}$ as a function of cycle number when cycled at 260 mA/g between 3 V - 0.01 V vs $\text{Na}^{+/0}$. (C) Rate capability tests for $\text{TiO}_x(\text{OH})_y\text{-400}$.

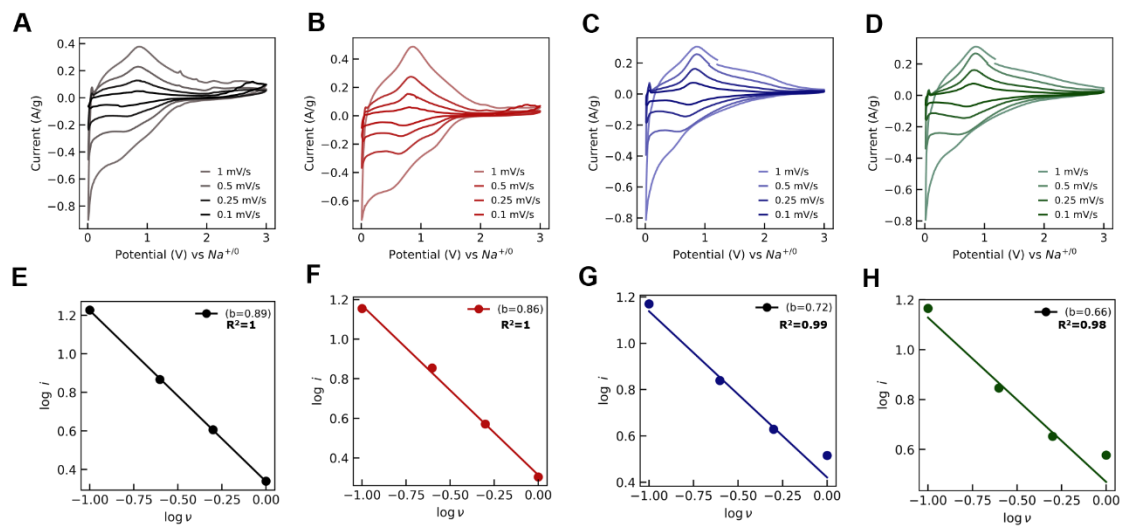


Figure S7. Cyclic voltammograms for (A) $\text{TiO}_x(\text{OH})_y$ -RT, (B) $\text{TiO}_x(\text{OH})_y$ -200, (C) $\text{TiO}_x(\text{OH})_y$ -400, and (D) $\text{TiO}_x(\text{OH})_y$ -600 (scan rates as indicated); (E) corresponding $\log i$ vs. $\log v$ plots for $\text{TiO}_x(\text{OH})_y$ - T_{anneal} (b-values were obtained from the slope of each linear fit) as shown.

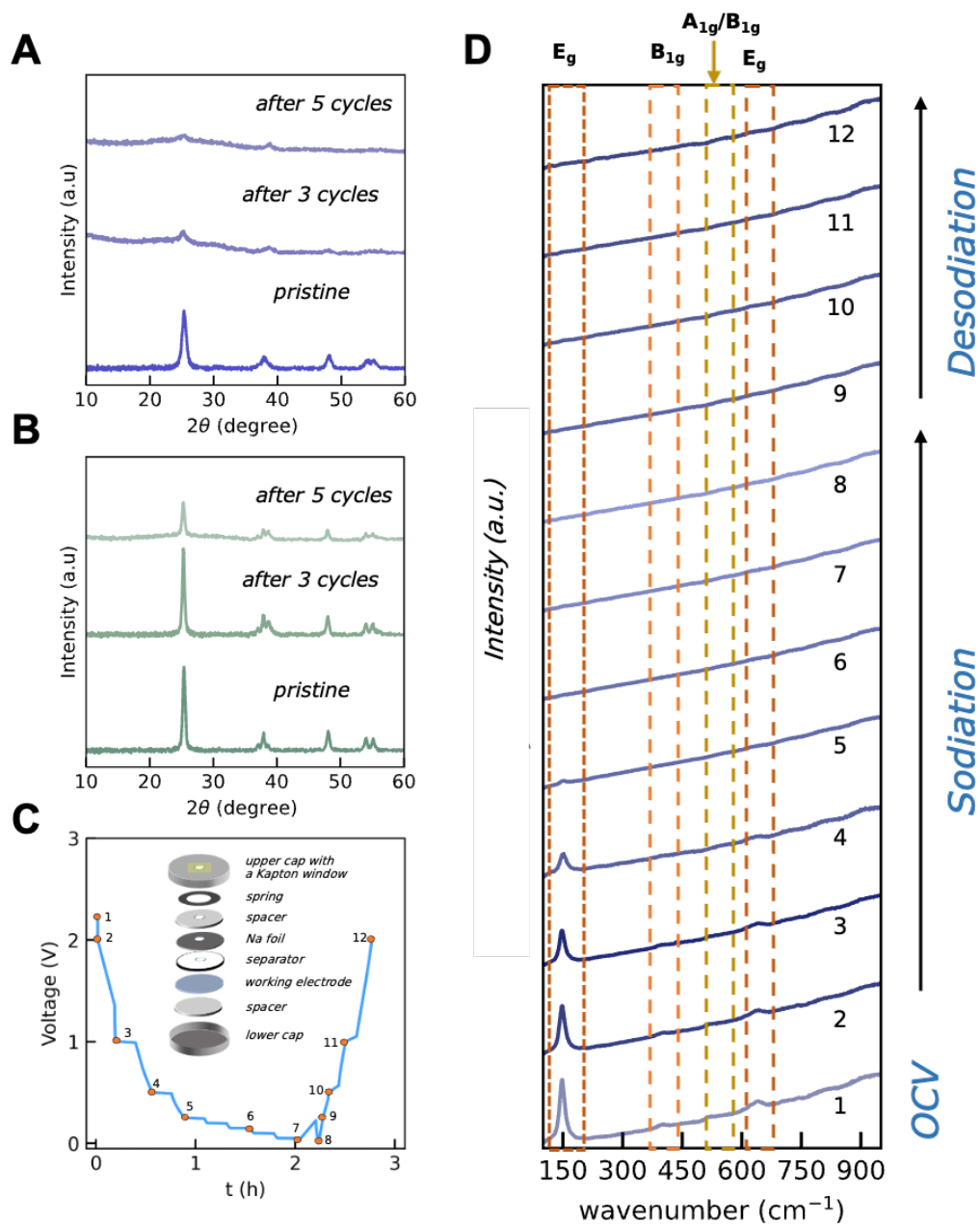


Figure S8. pXRD data for (A) $\text{TiO}_x(\text{OH})_y\text{-400}$ (B) $\text{TiO}_x(\text{OH})_y\text{-600}$ after 3rd and 5th cycle respectively (GCD at 260 mA/g). (C)-(D) In situ Raman spectra of $\text{TiO}_x(\text{OH})_y\text{-400}$ electrode when cycled at 260 mA/g (the cell setup is shown as an inset).

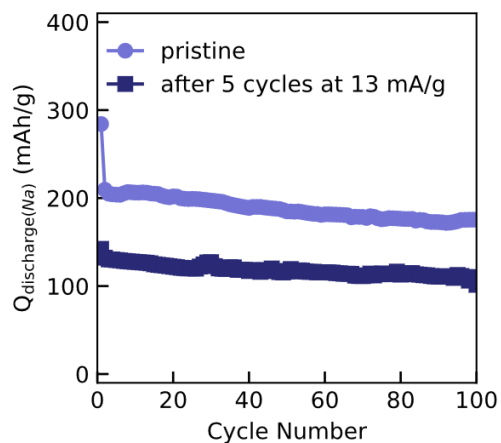


Figure S9. Comparative cycling performance for $\text{TiO}_x(\text{OH})_y\text{-400}$ at 260 mA/g, with and without 5 initial cycles at 13 mA/g.

Table S1. Water content in $\text{TiO}_x(\text{OH})_y\text{-T}_{\text{anneal}}$ as determined from TGA.

S. No.	Sample	Water content
1	$\text{TiO}_x(\text{OH})_y\text{-RT}$	0.78
2	$\text{TiO}_x(\text{OH})_y\text{-200}$	0.43
3	$\text{TiO}_x(\text{OH})_y\text{-400}$	0.10
4	$\text{TiO}_x(\text{OH})_y\text{-600}$	0.04